Journal of Catalysis 280 (2011) 255–263

Contents lists available at ScienceDirect

Journal of Catalysis

journal homepage: www.elsevier.com/locate/jcat

Decoration with ceria nanoparticles activates inert gold island/film surfaces for the CO oxidation reaction

Zheng Zhou, Maria Flytzani-Stephanopoulos *, Howard Saltsburg *

Department of Chemical and Biological Engineering, Tufts University, Medford, MA 02155, USA

ARTICLE INFO

Article history:
Received 4 January 2011
Revised 24 March 2011
Accepted 25 March 2011
Available online 22 April 2011

Keywords:
Gold
Ceria
CO oxidation
Interfacial gold atoms
Inverse structure

ABSTRACT

Ceria nanoparticles (<5 nm) were deposited on a polycrystalline gold film supported on SiO_2/Si substrate in an e-beam apparatus, and the catalytic activity of the inverse CeO_2/Au structure for the CO oxidation reaction was evaluated at ambient pressure in a recycle reactor. The gold film contained large crystal grains (lateral size in tens and hundreds of nanometers) and was nearly inert. CeO_2 nanoparticles deposited directly on the silicon substrate were also inert. However, decoration of the gold film with CeO_2 nanoparticles produced an activity enhancement of three orders of magnitude. This induced activation of the gold surface atoms at the interface with ceria nanoparticles was independent of the grain size of the gold film but proportional to the amount of CeO_2. No visible reconstruction of the Au surface upon ceria deposition was found by TEM. XPS analysis identified a high concentration of Ce^{3+} in the ceria nanoparticles, but was not useful in identifying the state of the interfacial gold atoms. In stability studies, it was found that deactivation was accompanied by a decrease in the Ce^{3+} concentration. The Au interfacial atom-TOF of the inverse CeO_2/Au film structures and Au/CeO_2 nanoparticles was similar, as was the apparent activation energy, E_{app} = 49 ± 9 kJ/mol, indicating a common reaction mechanism.

1. Introduction

Dispersing nanoscale gold particles on metal oxides provides active catalysts for many reactions [1,2], including the low-temperature CO oxidation [3]. Despite numerous studies of gold as a catalyst, the origin of the exceptional activity associated with nanoscale gold, even for the CO oxidation reaction, remains unclear. It has been proposed that the enhanced activity of nanoscale gold for CO oxidation is due to the high number of under-coordinated gold atoms [4] or a quantum size effect [5] corresponding to the gold particle size reduction. The coordination number (CN) of gold atoms was reported to affect the binding energy of CO and O_2: molecules could bind more easily on gold with low CN [4,6]. Surface flatness [7] and the angle of the surface gold atoms [8] were also reported as other factors that affect the binding energy of CO. In addition, theoretical studies of the binding of O_2 on free gold clusters and gold clusters adsorbed on Au (1 1 1) slabs showed similar energetics, indicating that it is the localized electronic properties rather than the overall electronic properties which affects the activity [7,9]. Other studies attributed the enhancement in activity to the synergistic effect of the active supports and gold [10,11]. The critical step of oxygen activation was found to be facilitated by electron-rich gold as a result of electron transfer from the oxide support (TiO_2 [12] and MgO [13,14]) to the gold and by the defects on the support itself [15].

To explain the enhanced activity related to the size reduction and the active support, a number of studies have been carried out to compare activities for the gold-catalyzed CO oxidation on active and inert supports. With the particle size of gold kept to similar values, the difference in activities of gold supported on inert and active supports was attributed to a synergistic effect between gold and the active support [16–18]. Nevertheless, conflicting conclusions are found in the literature. Okumura et al. reported no appreciable effect from the support (SiO_2 or TiO_2) as long as the gold is dispersed at the nanometer scale (2–6 nm) and has strong interaction with the support [17]. On the other hand, Herranz et al. studying gold in the same size range found a temperature-dependent promotion effect from the active support, TiO_2, and reported that Au/TiO_2 was about five times more active than Au/SiO_2 at 90 °C [16]. In general, it is hard to compare results from different groups even for catalysts of the same type and similar gold particle size, due to the differences in the preparation methods, operating conditions [17,18] and catalyst pretreatment protocols. It is worth mentioning that an oxidizing treatment has been reported to enhance the activity of gold fine powder, probably by oxidizing gold atoms on the particle surfaces [19]. Nano-sized gold might be more sensitive to the oxidizing treatment, and the variants of pretreatments could result in different conclusions as to the effect of the

* Corresponding authors.
E-mail addresses: maria.flytzani-stephanopoulos@tufts.edu (M. Flytzani-Stephanopoulos), howard.saltsburg@tufts.edu (H. Saltsburg).

0021-9517/$ - see front matter © 2011 Elsevier Inc. All rights reserved.
doi:10.1016/j.jcat.2011.03.023

support on the gold activity [17,19]. This makes it really challenging to delineate the contribution from the support, if any, and determine the nature of the active sites.

Alternative approaches to studying the nature of the active sites and the gold–support interactions have been reported. They involve using gold with extended surfaces such as Au single-crystal films and large-size polycrystalline powders. In these studies, gold with large dimension was decorated with metal oxide particles of a few nm in size; this structure has been described as an "inverse" Au/metal oxide structure relative to conventional catalysts where metal oxide is in excess. In an early report, Vannice's group showed that TiO_2 activates inert gold powder with large particle size (10 μm) for the CO oxidation reaction [20]. Nano-sized ceria deposited on a Au(1 1 1) single-crystal was found to be active for the water–gas shift reaction [21]. In both cases, before decoration with the metal oxide, the gold surface was inactive, as shown by experimental measurements [20] and in agreement with DFT calculations [21]. Therefore, the increased activity after decorating the gold surface with metal oxide particles is direct evidence of the oxide effect on gold. The single-crystal inverse structures permit one to use in situ spectroscopy aimed at identifying potential electronic effects and the new adsorption sites created upon the metal–oxide contact. Liu and Vannice [22] characterized the CO and O_2 adsorption using TPD, AES and XPS on both the bare gold surface and that subsequently decorated with TiO_2. However, in their study, no specific properties related to the interfacial sites could be identified. We recently studied the CO oxidation reaction at ambient pressure on a well-controlled Au/CeO_2 multilayered structure (called nanotower) [23], which allows one to differentiate reaction on the metal surface from that at the Au/CeO_2 interface. The CO oxidation rate was found to scale with the total length of the Au/CeO_2 interface for nanotowers with the same total Au and CeO_2 surface areas. TEM investigations revealed highly stressed films in the nanotowers, which are temperature- and film thickness-dependent. The stress change upon heating was proposed to be one of the causes of catalyst deactivation [23].

There are still gaps in our understanding of the findings on both the inverse Au/metal oxide structures and the conventional metal oxide-supported nanoscale gold catalysts. Most studies on extended gold surfaces were conducted under high vacuum. The information obtained under such conditions may not be directly applicable to catalyst response under higher pressure conditions, including different surface adsorbates, such as hydroxyl groups and/or water [16]. The inverse structures using polycrystalline gold surfaces, typically in particulate form, have been examined under ambient pressure. A promotion effect was observed unambiguously using the inverse structure of TiO_2–Au powder [20]. However, the activity was lower on TiO_2–Au powder than that on oxide-supported nanoscale gold [20]. Due to the lack of further information, the existence and the relative importance of the different reaction channels has not been established, a significant drawback when designing an effective catalyst.

To study these questions, a new inverse structure of Au/metal oxide was evaluated in this work. Ceria was selected as a catalytically active (oxygen-defect-rich) oxide and silica as an inert oxide. Ceria-decorated Au polycrystalline films were prepared to study the support effect at ambient pressure bridging the gap between the surface science studies on extended gold surfaces and the conventional Au/CeO_2 catalysts with gold nanoparticles deposited on ceria. The inverse structures using polycrystalline gold films on which the cerium oxide islands were deposited were prepared by evaporation using an e-beam apparatus and were tested for activity at ambient pressures in a recycle reactor described previously [23]. A gold film was deposited on a Si (1 0 0) substrate that had 100 nm of thermally grown oxide. This was tested for activity and was subsequently decorated with metal oxide (CeO_2 or SiO_2) to study the potential promotion effect of the metal oxide. The film growth was monitored using a quartz crystal microbalance that allows good control of the thicknesses of the gold film and of the active (CeO_x) or inert (SiO_2) oxide layers or islands deposited on the surface of the gold film. The change in the Au properties after deposition of the metal oxides can be monitored and correlated with the ensuing activity. Using this structure, the effect of CeO_2 (active oxide) was studied and compared to the effect of SiO_2 (inert oxide) for different size (thickness) gold films. The activity of gold at the interface with ceria in the inverse structures was compared to that of supported nano-sized gold catalysts described in the literature.

2. Experimental

2.1. Catalyst preparation

Polycrystalline Au films with mass equivalent film thicknesses of 4.5 nm and 20 nm (measured with a quartz crystal microbalance), referred to hereafter as Au (4.5 nm) and Au (20 nm), were studied. The variation in the film thickness was to simulate the size variation of gold particles on oxide supports. The Au films and the metal oxide islands (CeO_2 and SiO_2) were deposited on SiO_2/Si (1 0 0) substrates (3″ in diameter) using a multisource e-beam vapor deposition system (Ebeam, PAK-8, Sloan). Pellet Au (99.99%), CeO_2 (99.9%, AITHACA Chemical Corp.), and SiO_2 (99.99%, Alfa Aesar) were used as sources. The base pressure was 10^{-6} Torr, and the deposition rates were 0.1 nm/s for Au films and 0.01 nm/s for the metal oxide decorations. The amount deposited was monitored using a quartz crystal microbalance (QCM) placed close to the substrate. The substrate was kept at room temperature at the beginning of the deposition. In studying the effect of CeO_2 and SiO_2 decoration, the undecorated gold film was tested in a separate recycle reactor under ambient atmosphere before being transferred back to the vacuum chamber for a second deposition of CeO_2 or SiO_2.

2.2. Characterization

The gold films were characterized using X-ray diffraction (XRD, Rigaku RU300, K_α) and scanning electron microscopy (SEM, Ultra55, Zeiss) of the film texture including the crystal structure and the topography. In XRD, the X-ray generator and the detector rotated with respect to the normal of the substrate (the direction of the film thickness), so that the crystalline information across the film thickness was collected. The ceria decoration was studied using high-resolution transmission electron microscopy (TEM JEOL 2010).

X-ray photoelectron spectroscopy (XPS) was used to determine the surface atomic ratio and the oxidation state of Au and Ce. The X-ray source was Al K_α (15 kV, 10 mA) and the pass energy was 20 eV. Most of the samples contained ceria, and the spectra were referenced to the highest binding energy peak of Ce^{4+} $d_{3/2}$ at 916.5 eV [24–26]. In all samples, the binding energy of O 1s in SiO_2 of the substrate layer was found to be 532.6 eV with an uncertainty in the peak position of ±0.2 eV. Therefore, 532.6 eV was used as the charging reference when CeO_2 was absent in the sample. The coverage of the gold films on the SiO_2 substrate [Au/Si] and the ceria coverage on the gold films [Ce/Au] were determined using Eqs. (1)–(4). In the inverse structure, ceria was deposited on the top of the gold film. Therefore, only the bare gold film (gold film without any decoration) can be used in calculating the gold film coverage. In calculating [Ce/Au], the value of [Au/Si] from a bare gold film made under the same conditions was used for a better estimate, since ceria nanoparticles also grew on the substrate surface as observed by TEM (Fig. 1).

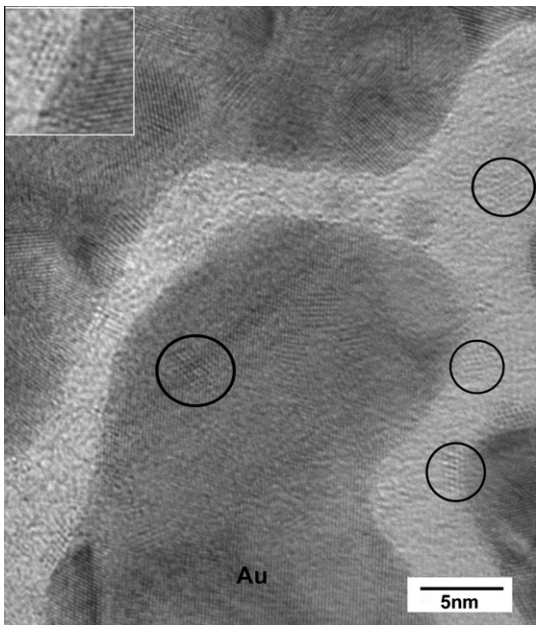

Fig. 1. Bright-field images of TEM for ceria nanoparticles deposited on discontinuous gold film. Some of the ceria nanoparticles are circled. Identification was based on the lattice fringes (~0.24 nm for Au (1 1 1) and ~0.32 nm for CeO_2 (1 1 1)). The inset is 5 nm by 5 nm. The TEM grid was used as substrate instead of the SiO_2/Si (1 0 0). No obvious effect was found from the substrate to the growth of Au (4.5 nm) film as comparing the SEM image of Au grown on silicon substrate and the TEM image of gold on carbon film.

$$N_x = I_x/\mathrm{RSF}_x \quad (1)$$

$$[\mathrm{Au/Si}] = N_{\mathrm{Au}}/(N_{\mathrm{Au}} + N_{\mathrm{Si}}) \quad (2)$$

$$[\mathrm{Ce}] = N_{\mathrm{Ce}}/(N_{\mathrm{Ce}} + N_{\mathrm{Au}} + N_{\mathrm{Si}}) \quad (3)$$

$$[\mathrm{Ce/Au}] = [\mathrm{Ce}]^*[\mathrm{Au/Si}] \quad (4)$$

where N_x is the number of surface atoms of element x; I_x is the peak area of a specific peak; RSF is the relative sensitivity factor (6.25 for Au 4f, 8.808 for Ce 3d, and 0.324 for Si 2s).

A quantitative analysis of Ce^{3+} concentration was conducted by curve fitting the Ce 3d spectra. After removing spectra with the Shirley background, the resultant curve was fitted with ten peaks as described in Refs. [26–29] with four peaks attributed to Ce^{3+} (v_0, v', u_0, and u') and the other six attributed to Ce^{4+} (v, v'', v''', u, u'', and u'''). The Ce^{3+} concentration [Ce^{3+}] was calculated using Eqs. (5)–(7) as described in [27]:

$$I_{Ce^{3+}} = I_{v0} + I_{v'} + I_{u0} + I_{u'} \quad (5)$$

$$I_{Ce^{4+}} = I_v + I_{v''} + I_{v'''} + I_u + I_{u''} + I_{u'''} \quad (6)$$

$$[Ce^{3+}] = I_{Ce^{3+}}/(I_{Ce^{3+}} + I_{Ce^{4+}}) \quad (7)$$

The variability in quantitative analysis of [Ce^{3+}] due to vacuum conditions in the XPS chamber was within 2% over the samples tested at different times.

2.3. Catalytic activity measurement

Activity measurements were conducted using the recycle reactor. The reactant gas mixture was circulated within the reactor loop using a metal bellows pump. A capillary connected to the loop was used to leak trace amounts of gas to a quadrupole mass spectrometer (QMS), where the gas concentration was analyzed in real time [23]. O_2 and CO reactants were injected sequentially into the reactor gas stream (initially pure He). The time delay from injection to the response of the mass spectrometer (<10 s) is very small relative to the reaction time (a few minutes to a few hours). The measurement was conducted at 160 °C at ambient pressure, and the initial gas stream contained 1% CO and 2% O_2, balanced with He. To compare the activity between samples, the initial reaction rate was obtained by fitting the concentration–time curve. A typical curve is shown in Fig. 2a. For samples with low activity, an extended reaction time as long as 10 h was used. Since all the catalysts were prepared as thin films on flat substrates, the activity data were related to the geometrical surface of the substrate supporting the catalyst and were expressed as mol CO_2/s/cm^2.

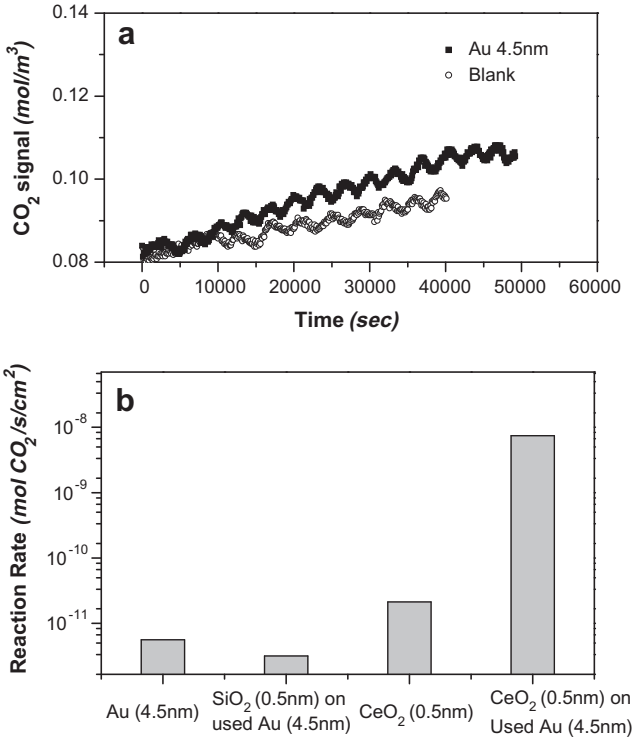

Fig. 2. CO_2 concentration with test time for Au (4.5 nm) film and blank reactor (a) and CO oxidation activity of various samples (b). CeO_2 was deposited on used Au film (1%CO–2%O_2–He, 160 °C, 7 h). The CO_2 signal increase from the blank reactor test was subtracted in calculating the reaction rates.

3. Results and discussion

3.1. Texture of gold films

The texture of the gold films, including the grain size and the film topography, can be altered by several factors such as the substrate temperature, the deposition rate during deposition, the film thickness, and the post-deposition thermal treatment. The substrate temperature and the deposition rate were fixed during the deposition. Therefore, the major factors that can change the grain size of the gold films are the deposited film thickness and the annealing during the activity test. These variables were studied using SEM and XRD (Table 1).

3.1.1. Grain size change with film thickness

XRD confirmed the presence of polycrystalline gold in all samples, as expected for films grown on substrates at low-temperatures. The grain size along the direction of the substrate normal was found to be 5 nm and 22 nm for the designed film thickness

Table 1
Properties of Au films deposited on SiO_2/Si (1 0 0) surfaces.

[a]Equivalent film thickness (nm)	Condition	Grain size (XRD) (nm)	Atomic% (XPS) Au/(Au + Si) × 100[c]
4.5	As-deposited	5.5	70
4.5	[b]160 °C Used	13	48
20	As-deposited	22	100
20	[b]160 °C Used	27	100

[a] The equivalent film thickness was estimated by the mass deposition recorded by a quartz crystal microbalance.
[b] The sample was tested at 160 °C for 7 h, the gas mixture was 1%CO–2%O_2–He.
[c] The XPS analysis was performed on the ceria-free gold surfaces.

of 4.5 nm and 20 nm, respectively. The increase in the crystal grain size with the film thickness showed the gold film was well crystallized during deposition and gold crystal size was proportional to the film thickness.

The topography of as-deposited gold is shown in Fig. 3. With 4.5 nm equivalent film thickness (Fig. 3a), the gold film is discontinuous and island shaped, showing film growth at the coalescence stage. The shape of the islands is elongated, with the longer dimension in the range of 80–150 nm and the shorter dimension over 10 nm. In between the big islands, occasionally small rounded islands with lateral size of 8–15 nm in diameter can be seen. The gold film covers about 70% of the substrate surface. With increase in the film thickness, the gold film becomes continuous. With 20 nm equivalent film thickness (Fig. 3c), the substrate is completely covered. The film continuity was confirmed by the XPS survey spectra in which no Si signal from the substrate was detected. The lateral size of the gold domain on the surface is slightly larger than that of Au 4.5-nm films, probably due to crystallization of gold horizontally with increased film thickness. Combining the information from SEM and XRD studies on as-deposited gold, it is reasonable to conclude that the grain size in the Au 20-nm film is larger than that in Au 4.5-nm film and that it is appropriate to use the varying film thicknesses to simulate gold particles of various sizes.

3.1.2. Grain size change upon heating

Aggregation and recrystallization were observed for the Au films upon heating. For as-deposited Au (4.5 nm), after conducting an activity test at 160 °C for 7 h, the lateral size of the Au islands almost doubled (Fig. 3b). The grain size normal to the film also grew. XRD showed the grain size along the substrate normal increased to 13 nm, which was almost triple its nominal (mass-based) size. The gold film coverage was reduced from 70% to 48% accordingly. The texture remained stable upon extended activity measurement: no further increase in grain size was found for the gold film. Recrystallization was also found for the continuous Au (20 nm) films. The grain size increased to 27 nm along the substrate normal after activity measurement. However, no Si signal from the substrate was detected using XPS, indicating that the gold film remained continuous. It is well known that films grown on substrates at low-temperatures are less well crystallized than those grown on substrates at elevated temperatures [30]. Since the polycrystalline gold films prepared in this work were grown on substrates at lower temperature while tested at higher temperatures, it is reasonable that the grain size increased after the activity measurement.

3.2. Ceria decoration

Ceria particles also grew in a 3D mode. TEM showed that ceria grew into small particles of 3–4 nm in diameter (Fig. 1). When deposited onto a discontinuous 4.5-nm gold film, ceria nanoparticles were found to grow on both the gold islands and the exposed silica substrate in between the gold islands. The ceria nanoparticles grown at the edge of the gold islands show a nearly abrupt interface between gold and ceria. No obvious surface roughening was found for the gold surface around the ceria nanoparticles, indicating the impact of ceria was not hard enough to cause a local morphology change of gold.

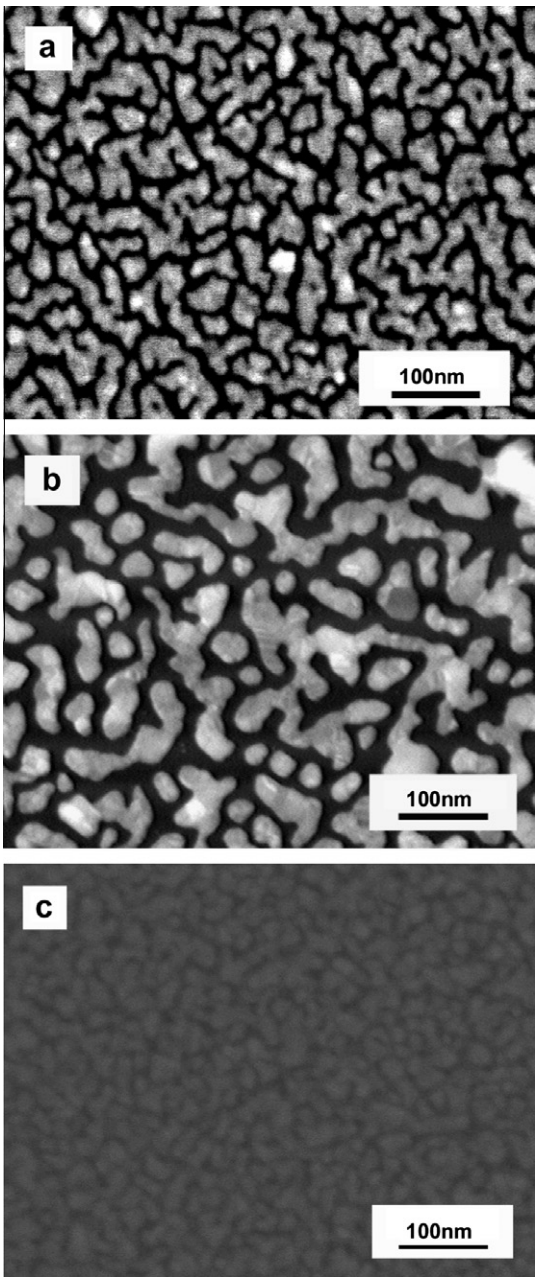

Fig. 3. SEM images of e-beam deposited gold. Au film: (a) 4.5 nm (fresh); (b) 4.5 nm (used, 160 °C, 7 h); (c) 20 nm (fresh).

3.3. XPS

The as-deposited ceria nanoparticles were highly defective, but they were partially oxidized during the activity measurement. The typical Ce 3d spectra for a pair of as-prepared and tested samples are shown in Fig. 4a. The characteristic peaks for Ce^{3+} (u' and v') were less intense on the used sample. The coverage of ceria

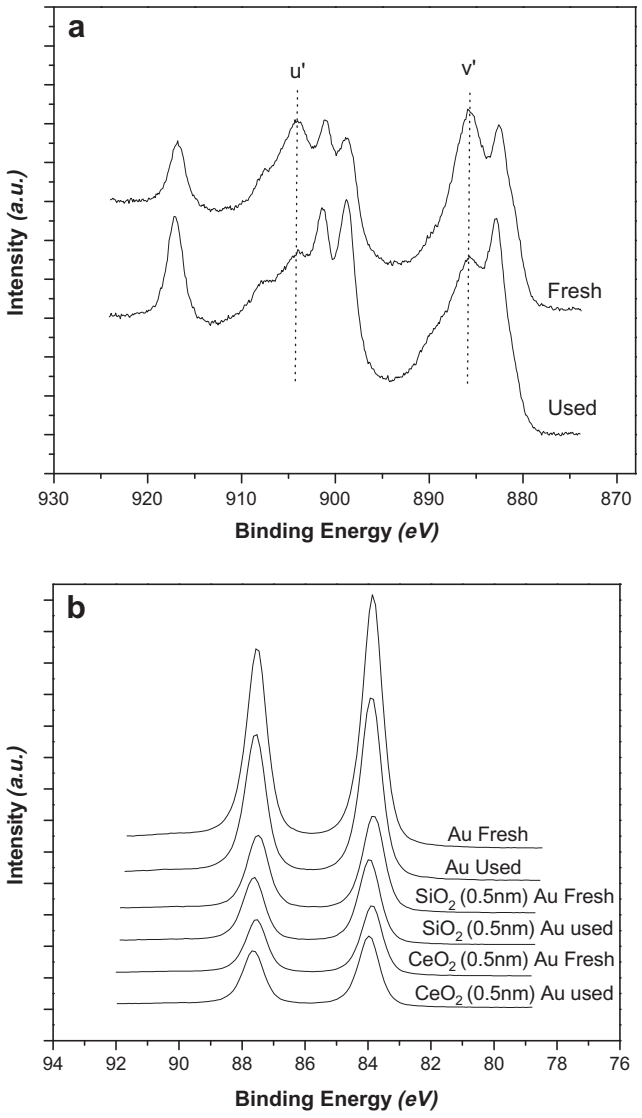

Fig. 4. XPS for Ce 3d (a) and Au 4f (b) on various gold films. Fresh: as-deposited film. Used: sample was tested for the CO oxidation reaction at 160 °C for 7 h.

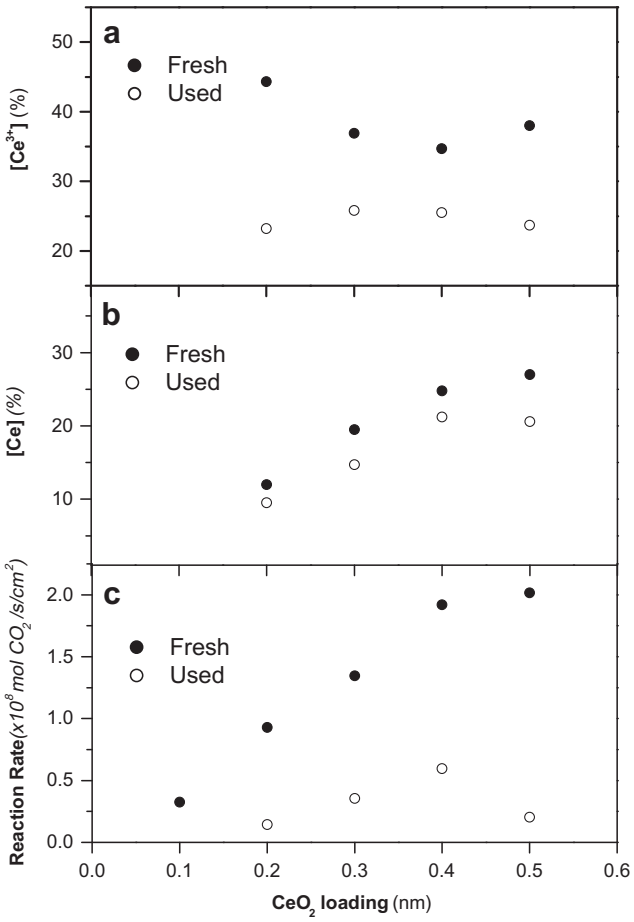

Fig. 5. Ce^{3+} concentration (a) and CeO_2 coverage (b) as estimated from XPS and CO oxidation activity (c) as a function of ceria loading on CeO_2 decorated Au film (4.5 nm, fresh), 160 °C, 1%CO–2%O_2–He bal. Fresh: as-deposited samples. Used: Samples tested for 7 h.

([Ce]), based on atomic ratios from the XPS analysis, increased almost linearly with the ceria decoration amount (Fig. 5b). The coverage decreased about 3–5% for the used samples, suggesting slight sintering or contraction of ceria during the reaction. Quantitative analysis of Ce 3d spectra found high Ce^{3+} concentrations of 36–38% (Table 2) for the as-deposited ceria, probably originating from partial decomposition of ceria during e-beam deposition. There was no extra gas-phase oxygen during the deposition. The defect concentration [Ce^{3+}] decreased to 24–26% for samples tested under oxygen-rich conditions.

The binding energy of Au 4f centered at 83.9 eV for all samples (Fig. 4b), which is in the range of values reported for bulk gold (83.8–84.0 eV) [31]. The binding energy did not change upon further deposition of SiO_2, as was expected for Au/SiO_2 catalysts due to lack of interaction between gold and inert SiO_2. However, after deposition of ceria, no additional change in either the peak shape or the peak position was found. Although a large part of gold surface (13–27%) was in contact with the ceria, the XPS signal from this part of gold might be attenuated or blocked by the ceria nanoparticles, and the Au spectra remain unchanged due to the preponderance of the uncovered (ceria-free) gold surface.

Table 2
XPS analysis of the ceria coverage and Ce^{3+} concentration for CeO_2 (0.5 nm)-decorated gold surfaces.

Sample	[Ce][a] (%)	[Ce/Au][b] (%)	[Ce^{3+}][c] (%)
CeO_2 on used Au 4.5 nm, Fresh	30	14	38
CeO_2 on used Au 4.5 nm, Used	28	13	26
CeO_2 on fresh Au 4.5 nm, Fresh	27	20	38
CeO_2 on fresh Au 4.5 nm, Used	21	15	24
CeO_2 on fresh Au 20 nm, Fresh	27	27	36
CeO_2 on fresh Au 20 nm, Used	27	27	25

"Fresh" indicates that the samples were as-prepared and "used" indicates that the samples were tested under the same conditions for about 7 h.

[a] The value is calculated as Ce/(Ce + Au + Si) × 100% by XPS analysis of the surface atomic ratios.

[b] The value is from CeO_2% on the surface multiplied by the Au coverage from Table 1; 70% for fresh gold (4.5 nm) film, 48% for used gold (4.5 nm) film, 100% for gold (20 nm) film.

[c] Ce^{3+} concentration is estimated by curve fitting the Ce 3d spectra from XPS.

3.4. Catalytic activity measurement

3.4.1. Promotion by ceria deposition

The most effective dimension for conventional particulate gold catalysts for the CO oxidation reaction was reported to be below 5 nm [4,10]. With a lateral size of 20–100 nm, the catalytic activity of the gold islands of Au film (4.5 nm) is expected to be more like

that of bulk gold, which is only weakly active compared to nanoparticle gold [32]. To evaluate the catalytic properties of this type of gold, the CO oxidation activity of Au film (4.5 nm) was examined in the recycle reactor. The CO_2 concentration increased with time (Fig. 2a), showing that the bare gold was active. Similar results were observed on fine gold powder of 76 nm [19] and on a Au layer (8 nm) on SiO_2/Si (1 0 0) [33]. It was proposed that the fine gold powder contained more defects that can adsorb CO and it had better oxygen affinity than a Au (1 1 0) single-crystal [19], thus explaining its activity. The Au film (4.5 nm) prepared here by e-beam deposition was deposited at low-temperature, which could have increased its density of defects. For a Au film prepared under similar conditions, i.e. by vapor deposition onto a substrate at low-temperature, defect sites that could adsorb CO were reported, while no CO adsorption was found on a Au film deposited on substrates at high temperatures [30,34]. Therefore, despite the relatively large lateral dimension, there might be defects on our Au (4.5 nm) film that catalyze the reaction. Nevertheless, the activity was low as expected for gold islands with large lateral sizes.

The Au (4.5 nm) film was then decorated with ceria nanoparticles (0.5 nm in equivalent film thickness). After decoration, the activity on the sample was found to be three orders of magnitude higher (Fig. 2b). Although the ceria nanoparticles were very defective, this was not a good catalyst by itself. The same type of ceria nanoparticles, when grown on SiO_2 substrate, can be considered to be inert compared to the sample with both gold and ceria (Fig. 2b). Therefore, the enhanced activity of gold film upon ceria decoration and heating to the reaction conditions shows a dramatic activation of the gold at the interface with ceria. In addition, the activity scales with the ceria decoration amount. Several as-deposited Au (4.5 nm) films were decorated with various amounts of CeO_2 (0.1–0.5 nm in equivalent film thickness). The activity increased linearly with ceria loading (Fig. 5c). As found by XPS, the coverage of the ceria also increased with the loading (Fig. 5b), indicating that the ceria was well dispersed on the gold surface. With increased ceria coverage, more Au/CeO_2 interfaces were created, which could explain the linearly increased activity with ceria loading. In most supported gold catalysts, gold nanoparticles have only one side in contact with the metal oxide support. Adding more gold while keeping it dispersed increases the contact sites with the support, thus increasing the activity. The same argument can be made here for the inverse structure. Adding more ceria, while keeping it dispersed, increases the number of contact sites with the gold film; hence, the activity is increased.

A TEM study did not reveal any obvious distortion of the gold surface around ceria islands; instead, the ceria/Au interface was nearly abrupt (Fig. 1), indicating there was barely reconstruction of gold upon ceria deposition. Although formation of defects on the gold surface from the physical impact during ceria deposition was not reported, this may be possible due to the sensitive relationship between gold structure and its adsorption ability [7,8], which in turn affects the activity. To exclude this possibility, this effect was examined by substituting the impact material with an inert metal oxide (SiO_2). The activity measurement was repeated on a new Au film (4.5 nm). The sample was then decorated with vapor-deposited SiO_2 and tested again for the CO oxidation reaction. The activity measurement showed no enhancement from SiO_2 deposition (Fig. 2), indicating that the gold cannot be activated solely by impaction from an inert oxide deposition. However, it is possible that gold atoms have rearranged at the points of contact with the ceria upon being exposed to reaction conditions and became active. Lattice expansion with increasing Ce^{3+} concentration has been reported for ceria nanoparticles [35]. The ceria nanoparticles in this work were highly defective, containing up to 38% Ce^{3+}, which decreased during the oxidation reaction (Table 2), hence causing a contraction, i.e. a lattice parameter reduction. The lattice contraction in the ceria nanoparticles could impose a force to the underneath gold and cause tensile stress in gold at the interface, which in turn activated the gold. Since SiO_2 is a non-reducible metal oxide and cannot impose a force to the underneath gold as the defective ceria nanoparticles would upon oxidation, this may explain why the gold film was not activated by SiO_2 island decoration. Although stress due to the lattice mismatch between gold and metal oxide supports has been observed [36] and was proposed to be a factor that affects the catalytic activity of gold [37], the possible stress change posed by the mechanical force from the reducible metal oxide contraction/expansion during redox reactions was never fully studied. In conventional catalysts where gold is present as nanoparticles, this effect might be crucial to the catalytic activity. In surface science studies, reconstruction of Au (1 1 1) surface by atomic oxygen has been found by STM [38]. While a Au (1 1 1) single-crystal decorated with ceria was also studied using STM, no signs of gold reconstruction around the ceria decoration were reported [39]. Further investigation of the potential Au reconstruction at the interface is needed to elucidate this issue.

Activation of oxygen is considered to be the critical step in CO oxidation for gold-based catalysts [40]. XPS analysis showed the decorated ceria was highly defective, which has been reported to activate oxygen for the CO oxidation reaction in a previous study of Au supported on ceria nanoparticles [41,42]. On the other hand, it has also been reported that electron-rich gold atoms can activate oxygen by transfer of charge to the $2\pi^*$ orbital of oxygen, thus weakening the O—O bond [7,43]. Although the XPS analysis of Au 4f spectra showed no evidence of local charge changes in gold, the presence of ionic gold cannot be ruled out, especially since the electronic interaction, if present, is confined to the interfacial sites [44]. In the ceria-decorated Au film (4.5 nm), less than 0.3 ML of Au atoms were in contact with the ceria according to the ceria coverage estimated from XPS (Fig. 5b). Hence, the contribution of this part of gold to the spectra might have been disguised by the abundant metallic gold signal from the polycrystalline Au film. It is not clear at this point whether the oxygen was activated by the defective ceria, through the gold atoms at perimeter sites, or whether another mechanism becomes operative. Nevertheless, the exceptional enhancement of activity shows direct evidence of the reaction channel open at ceria-modified sites even on Au islands with large lateral sizes.

3.4.2. Effect of Au grain size and ceria defects

Extensive studies on the effect of gold grain size have been carried out, with focus on catalysts with gold particles smaller than 5 nm. An increase in activity has been observed with decrease in the gold particle size [10]. On the contrary, the catalytic properties of gold larger than 10 nm have drawn little attention due to their low activity. In the inverse structure, the gold films have relatively large grain size and a planar configuration, on which multiple ceria nanoparticles can be deposited and thus increase the active sites. The activity increased almost linearly with ceria loading, suggesting that multiple active sites can be created on a single gold grain by decorating with ceria nanoparticles. Further study of the effect of gold grain size was carried out using the inverse structures with the gold films of varied grain size.

The grain size of the gold films can be varied by changing the film thickness or by annealing the gold film at elevated temperature. Three types of gold films were studied: Au (4.5 nm, fresh), Au (4.5 nm, used), and Au (20 nm, fresh) with the grain sizes across the film thickness being 5 nm, 14 nm, and 22 nm, respectively. After depositing 0.5 nm of fresh ceria, all three gold films became active for the CO oxidation reaction, with Au (20 nm, fresh) showing the highest activity, and Au (4.5 nm, used) the least activity (Fig. 6.). However, the difference in activities was within a factor

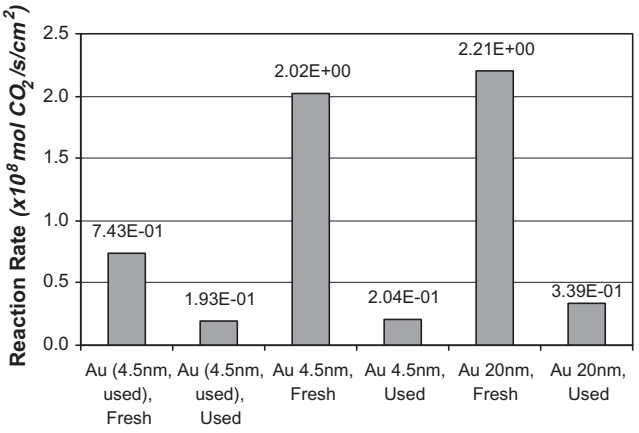

Fig. 6. Activity of CeO_2 (0.5 nm)-decorated fresh and used Au films (4.5 nm and 20 nm). The activities were normalized using the substrate area, reaction conditions: 1%CO–2%O_2–He, 160 °C. Fresh: initial activity. Used: activities measured on samples after for about 7 h of reaction.

of three, which was very small compared to the promotion effect from decoration of the gold film with ceria. Several factors other than the gold grain size variation can contribute to the difference in activity. First, the ceria coverage on Au surface is different in each sample even with the same nominal loading. As stated earlier, using the CeO_2 (0.1–0.5 nm)-decorated Au film (4.5 nm), the CO oxidation activity was proportional to the ceria coverage on Au ([Ce/Au]). Using a more defined multilayered Au/CeO_2 structure, it was recently shown that the activity for CO oxidation was proportional to the Au/CeO_2 interface length [23].

When ceria was deposited on a discontinuous film, such as Au (4.5 nm) film, a part of the ceria would land on the substrate (Fig. 1). On the contrary, when depositing ceria on a continuous gold film, such as the Au (20 nm) film, all the ceria would land on the gold surface (Fig. 1), thus increasing the number of active sites with the same ceria decoration amount. Therefore, taking the film continuity into account, the activity difference between samples with varied grain size would be further reduced. Second, the Au surface of a used sample is expected to be smoother than the as-deposited gold surface; therefore, the results suggest that the morphology of gold might play a role in the reaction, either by affecting the ceria dispersion or by itself. It has been reported that the surface flatness [7] and the angle of the surface gold atoms [8] could affect the catalytic activity by affecting the binding energy of CO. Nonetheless, compared with the promotion effect of adding ceria, which boosts the activity of the Au film about three orders of magnitude, varying the grain size of gold has only little effect on the activity.

Deactivation takes place on all samples. In the used samples, the activity dropped by about one order of magnitude (Fig. 6). As discussed earlier, the activity of the inverse structure CeO_2/Au scaled with the ceria coverage and was nearly unaffected by the grain size of gold. But the ceria coverage in the used samples was nearly unchanged compared to that of the fresh samples (Table 2). Therefore, neither the change in the ceria coverage nor the variation in the grain size in the gold films can account for the large activity loss. On the other hand, using XPS, we found that the ceria particles became less defective, as shown by a reduction in Ce^{3+} content in all the used samples (Table 2). The activities in the used samples still scaled with the ceria coverage (Fig. 5c), except for the one with 0.5 nm ceria loading. This could be explained by the relatively low Ce^{3+} concentration found in that sample. According to Guzman et al., nanocrystalline ceria can activate oxygen species at one-electron defect sites as active oxygen species for the CO oxidation reaction [45]. It would be interesting to correlate this with changes that have happened to gold at the Au/CeO_2 interface. In other studies, strong interaction between Au and CeO_2 (Au–O–Ce) was identified using EXAFS and XANES and was proposed to be related to the activity for the WGS reaction [46]. But the activation of OH which is crucial for the WGS reaction [47,48] may not involve the same sites as the dry CO oxidation. Hence, this issue remains unresolved.

3.4.3. Comparison of ceria/Au films with conventional nano-sized gold catalysts

For the bare Au film (4.5 nm), the TOF based on the exposed Au atoms was about two orders of magnitude lower than the most active Au/SiO_2 (Au particles 6.6 nm) catalyst reported in the literature (Table 3) [17]. This shows that although the polycrystalline gold deposited at room temperature contains some defect sites on the surface that can catalyze the CO oxidation reaction, the number of these defect sites is almost negligible compared with nanocrystalline gold. For the ceria-decorated gold films prepared and tested in this work, the apparent activation energy was 49 ± 9 kJ/mol (Fig. 7). This value agrees well with those reported for nano-sized gold catalysts [41,49], indicating similar reaction pathway for both large-sized gold and nano-sized gold. The rates measured on the ceria-decorated gold films in the range of 60–160 °C were extrapolated to lower temperature (303 K) and compared with those of nanoscale gold catalysts reported in the literature (Table 3). The TOF based on surface gold atoms was estimated for the ceria-decorated gold films, assuming a nearly flat gold surface. This activity was found comparable to that of the most active Au/CeO_x and Au/TiO_2 catalysts [41,42,49,50] with gold particle sizes in the range of 0.7–8 nm. This is understood as creation of active gold sites at the gold/ceria interfaces, which are equally effective, independent of the dimension of gold.

Estimates of TOF based on the interfacial gold atoms are listed in Table 3. Nearly the same activity is found as for gold nanoparticles supported on ceria despite the size variation in gold nanoparticles. The catalytic activity of these sites was affected by the defect concentration in ceria nanoparticles, but the effect of ceria may be understood as indirect, resulting in gold atoms that are charged (Au–O–Ce) or under-coordinated, so the interaction with the oxide is a way to promote the activation of gold. More detailed studies, especially atomic-resolution microscopy and STM studies, focusing on the atomic rearrangement of gold at the interface with ceria nanoparticles as the interface is exposed to different temperatures/adsorbates should be undertaken to fully resolve this question. In this effort, the inverse structures examined here will be particularly useful. Going a step further, the support oxide may be varied, with potentially minimal impact on the overall activity of gold. Indeed, as Table 3 shows, the interfacial Au atom-calculated TOF is not that different between ceria and titania. The support oxide may just serve to activate and preserve the gold atoms/ions that are the active sites for the CO oxidation reaction. In a recent paper, it was shown that unsupported, dendrimer-stabilized gold clusters in aqueous solution were as active as supported Au/TiO_2 for the oxidation of CO at ambient conditions [51].

4. Conclusions

The inverse structure of CeO_2/Au with ceria nanoparticles (<5 nm) on top of thin polycrystalline gold films was studied here for the CO oxidation reaction at ambient pressure and over a wide temperature range (60–160 °C). The polycrystalline gold films prepared be deposition on SiO_2/Si (1 0 0) substrates in an e-beam apparatus contain crystal grains with large lateral sizes (20–100 nm). Activity measurements on a nominally 4.5-nm-thick Au film showed the gold film to be active for the CO oxidation, but

Table 3
Comparison of CO oxidation activity of decorated Au film with nanoscale supported Au catalysts from the literature.

Catalyst	Au crystal size (nm)	CO:O_2	Reaction rate (mol CO/s/g_{Au})	T (K)	TOF (s^{-1}, Au at the surface)	TOF (s^{-1}, Au at the interface)	E_a (kJ/mol)	Ref.
Au (4.5 nm, fresh)	20 × 100 lateral size	1:2	/	433	[a] 3.4×10^{-3}	/	/	This work
Au/SiO_2	6.6	1:21	/	273/433	$2 \times 10^{-2}/3.2 \times 10^{-1}$	/	17	[17]
CeO_2 (0.5 nm) on Au (4.5 nm, fresh)	~20 × 100 lateral size 5.5 nm in depth	1:2	/	303	[a,b] 3.5×10^{-2}	[b,c] 2.2×10^{-1}	49 ± 9	This work
CeO_2 (0.5 nm) on Au (20 nm, fresh)	~20 × 100 lateral size 22 nm in depth	1:2	/	303	[a,b] 3.9×10^{-2}	[b,c] 2.4×10^{-1}	49 ± 9	This work
Au/CeO_2	0.7 (14 Au atoms)	1:1	/	303	5.6×10^{-2}	[d] 1.1×10^{-1}	54	[49]
$Au_{0.05}[Ce(La)]_{0.95}O_x$	8	1:1	2.4×10^{-5}	304	2.6×10^{-2}	4.5×10^{-1}	53.7	[41]
2.8% Au/CeO_2	4	1:19.8	1.06×10^{-4}	278	5.8×10^{-2}	4.9×10^{-1}	/	[42]
3.1% Au/TiO_2	2.9	1:21	6.45×10^{-4}	300	2.6×10^{-1}	1.6	27	[50]
Au/TiO_2	3.3	2:2	/	273	3.4×10^{-1}	2.4	29	[40]

[a] The polycrystalline gold film (4.5 nm) was taken as flat surface in calculation of the TOF, and the same number of gold atoms were assumed to be exposed on the surface as for a closely packed single-crystal (1 1 1) surface [38]; a gold atom density of $10^{15}/cm^2$ was used.
[b] TOF values extrapolated to 303 K.
[c] Hemispherical ceria nanoparticles with 3.5 nm diameter (as imaged by TEM) and ceria loading 0.5 nm (equivalent film thickness) were used in estimating the gold atoms at the Au/CeO_2 interface.
[d] A two-layer structure was assumed for the Au14 cluster, and the interfacial gold atoms were estimated to be 7/Au cluster.

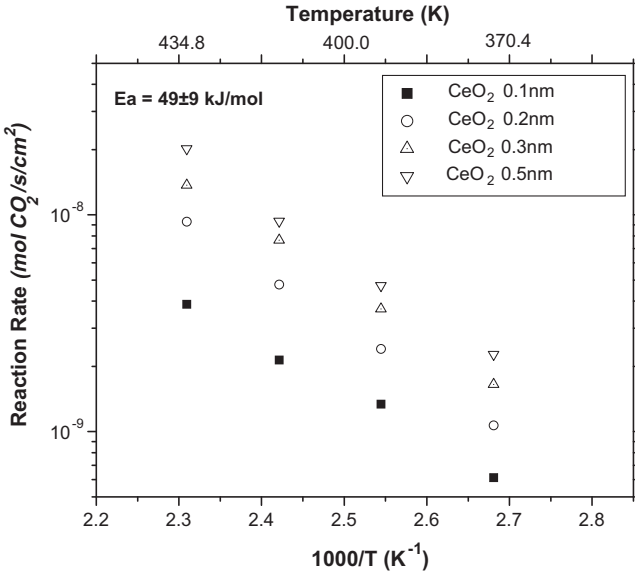

Fig. 7. Arrhenius-type plot for CO oxidation over ceria-decorated Au film (4.5 nm). The nominal size of a ceria film thickness based on calibrated loading is shown, but the actual size of ceria nanoparticles remains the same in all four samples; hence, the number of contact sites with the gold film increases linearly with the ceria loading. Reaction conditions: 1%CO–2%O_2–He.

the rate was extremely low, apparently because of very few active sites on the gold surface. Comparison of the activity to nano-sized gold catalyst (Au/SiO_2) from earlier reports confirmed that this type of gold lacked the number of active gold atoms present in nanocrystalline gold. Subsequent decoration of the tested gold surface (Au 4.5 nm) with ceria nanoparticles allowed the delineation of the effect of ceria without reference to gold grain size. An activity enhancement of about three orders of magnitude was observed after decorating the extended gold surfaces with 0.5 nm (nominal height) of ceria. The promoted activity was comparable to that reported for nanoscale Au/TiO_2 and Au/CeO_x with gold particle sizes of a few nanometers. Further investigation showed the reaction channel was independent of the gold lateral size, while the activity increased linearly with the amount of CeO_2 deposited. Deactivation was found on all the samples accompanied by the loss of Ce^{3+} in the ceria nanoparticles. These results suggest that there is a reaction channel activated by Ce^{3+}-rich ceria nanoparticles, probably at the interface of ceria particles and gold. With less than 30% of the gold surface occupied by ceria, the gold film shows activity comparable to 14-atom clusters of gold deposited on CeO_2 surfaces [49].

These results bridge the gap between studies on gold with different size ranges, indicating that the gold atoms that do the CO oxidation catalysis are very few; they are probably greatly uncoordinated and partially charged; for example, at the interface with the deposited ceria nanoparticles. So the optimal "size" of gold is not the issue; rather, the optimal "state" of gold may be a more proper distinction for the active sites. While we studied the electronic effect in the interaction of ceria NPs on the gold islands, we used XPS from which the information we could get was minimal, at least with reference to the gold active state. We were of course able to measure the indirect effect of ceria oxidation (loss of Ce^{3+}) on the activity. TOFs, calculated here on the basis of interfacial activated gold atoms, are in excellent agreement with the Au NP/ceria and other oxide supports, and the apparent activation energy is similar, 49 ± 9 kJ/mol. This indicates that the same reaction mechanism, involving the same type of gold atoms/ions is operating in all cases. Time-resolved, atomic-resolution microscopy work is needed to study the local structure at the gold/ceria interface during the catalytic reaction to further bridge the findings between the inverse CeO_2/Au structure and the nano-sized gold on ceria.

Acknowledgments

This work was supported by NSF under NIRT Grant 0304515 and the DOE/Basic Energy Science under Grant DE-FG02-05ER15730. The authors would like to thank Kurt Broderick (Microsystems Technology Laboratories at Massachusetts Institute of Technology) for the help with sample preparation, Dr. Heiner Jaksch (Carl Zeiss NTS) for the contribution on the SEM images, and Drs. Yong Zhang and Elisabeth Shaw (Center for Materials Science and Engineering, Massachusetts Institute of Technology) for their help with the TEM and XPS sample characterization.

References

[1] G.J. Hutchings, Catal. Today 72 (2002) 11.
[2] G.C. Bond, D.T. Thompson, Catal. Rev.: Sci. Eng. 41 (1999) 319.
[3] M. Haruta, N. Yamada, T. Kobayashi, S. Iijima, J. Catal. 115 (1989) 301.
[4] N. Lopez, T.V.W. Janssens, B.S. Clausen, Y. Xu, M. Mavrikakis, T. Bligaard, J.K. Nørskov, J. Catal. 223 (2004) 232.
[5] M. Valden, X. Lai, D.W. Goodman, Science 281 (1998) 1647.
[6] N. Lopez, J.K. Norskov, J. Am. Chem. Soc. 124 (2002) 11262.
[7] G. Mills, M.S. Gordon, H. Metiu, J. Chem. Phys. 118 (2003) 4198.

[8] G. Mpourmpakis, A.N. Andriotis, D.G. Vlachos, Nano Lett. 10 (2010) 1041.
[9] S.H. Overbury, V. Schwartz, D.R. Mullins, W. Yan, S. Dai, J. Catal. 241 (2006) 56.
[10] M. Haruta, Catal. Today 36 (1997) 153.
[11] A. Sanchez, S. Abbet, U. Heiz, W.-D. Schneider, H. Hakkinen, R.N. Barnett, U. Landman, J. Phys. Chem. A. 103 (1999) 9573.
[12] C. Steeve, M. Horia, J. Chem. Phys. 126 (2007) 104701.
[13] M. Sterrer, T. Risse, U.M. Pozzoni, L. Giordano, M. Heyde, H.-P. Rust, G. Pacchioni, H.-J. Freund, Phys. Rev. Lett. 98 (2007) 096107.
[14] C. Zhang, B. Yoon, U. Landman, J. Am. Chem. Soc. 129 (2007) 2228.
[15] J. Guzman, S. Carrettin, J.C. Fierro-Gonzalez, Y. Hao, B.C. Gates, A. Corma, Angew. Chem. Int. Ed. 44 (2005) 4778.
[16] T. Herranz, X. Deng, A. Cabot, P. Alivisatos, Z. Liu, G. Soler-Illia, M. Salmeron, Catal. Today 143 (2009) 158.
[17] M. Okumura, S. Tsubota, M. Haruta, J. Mol. Catal. A: Chem. 199 (2003) 73.
[18] S.D. Lin, M. Bollinger, M.A. Vannice, Catal. Lett. 17 (1993) 245.
[19] Y. Iizuka, T. Tode, T. Takao, K.-i. Yatsu, T. Takeuchi, S. Tsubota, M. Haruta, J. Catal. 187 (1999) 50.
[20] M.A. Bollinger, M.A. Vannice, Appl. Catal., B 8 (1996) 417.
[21] J.A. Rodriguez, S. Ma, P. Liu, J. Hrbek, J. Evans, M. Perez, Science 318 (2007) 1757.
[22] Z.M. Liu, M.A. Vannice, Catal. Lett. 43 (1997) 51.
[23] Z. Zhou, S. Kooi, M. Flytzani-Stephanopoulos, H. Saltsburg, Adv. Funct. Mater. 18 (2008) 2801.
[24] M.L. Trudeau, A. Tschöpe, J.Y. Ying, Surf. Interface Anal. 23 (1995) 219.
[25] A. Laachir, V. Perrichon, A. Badri, J. Lamotte, E. Catherine, J.C. Lavalley, J.E. Fallah, L. Hilaire, F.l. Normand, E. Quéméré, G.N. Sauvion, O. Touret, J. Chem. Faraday Trans. 87 (1991) 1601.
[26] F. Larachi, J. Pierre, A. Adnot, A. Bernis, Appl. Surf. Sci. 195 (2002) 236.
[27] F. Zhang, P. Wang, J. Koberstein, S. Khalid, S.-W. Chan, Surf. Sci. 563 (2004) 74.
[28] D. Creaser A, P.G. Harrison, M.A. Morris, B.A. Wolfindale, Catal. Lett. 23 (1994) 13.
[29] J.P. Holgado, R. Alvarez, G. Munuera, Appl. Surf. Sci. 161 (2000) 301.
[30] D.L. Smith, Thin-Film Deposition: Principles and Practice, McGraw-Hill, New York, USA, 1995.
[31] N.H. Turner, A.M. Single, Surf. Interface Anal. 15 (1990) 215.
[32] G.C. Bond, D.T. Thompson, Gold Bull. 33 (2000) 41.
[33] K. Frey, A. Beck, G. Peto, G. Molnar, O. Geszti, L. Guczi, Catal. Commun. 7 (2006) 64.
[34] P. Dumas, R.G. Tobin, P.L. Richards, Surf. Sci. 171 (1986) 579.
[35] L. Wu, H.J. Wiesmann, A.R. Moodenbaugh, R.F. Klie, Y. Zhu, D.O. Welch, M. Suenaga, Phys. Rev. B: Condens. Matter. 69 (2004) 125415.
[36] S. Giorgio, C.R. Henry, B. Pauwels, G. Van Tendeloo, Mater. Sci. Eng. A 297 (2001) 197.
[37] Y. Xu, M. Mavrikakis, J. Phys. Chem. B. 107 (2003) 9298.
[38] B.K. Min, X. Deng, D. Pinnaduwage, R. Schalek, C.M. Friend, Phys. Rev. B: Condens. Matter. 72 (2005) 121410.
[39] S. Ma, J. Rodriguez, J. Hrbek, Surf. Sci. 602 (2008) 3272.
[40] J.T. Calla, M.T. Bore, A.K. Datye, R.J. Davis, J. Catal. 238 (2006) 458.
[41] W. Liu, M. Flytzani-Stephanopoulos, J. Catal. 153 (1995) 317.
[42] S. Carrettin, P. Concepción, A. Corma, J.M.L. Nieto, V.F. Puntes, Angew. Chem. Int. Edit. 43 (2004) 2538.
[43] K. Honkala, H. Hakkinen, J. Phys. Chem. C. 111 (2007) 4319.
[44] C. Zhang, A. Michaelides, D.A. King, S.J. Jenkins, J. Am. Chem. Soc. 132 (2010) 2175.
[45] J. Guzman, S. Carrettin, A. Corma, J. Am. Chem. Soc. 127 (2005) 3286.
[46] W. Deng, A.I. Frenkel, R. Si, M. Flytzani-Stephanopoulos, J. Phys. Chem. C. 112 (2008) 12834.
[47] Q. Fu, H. Saltsurg, M. Flytzani-Stephanopoulos, Science 301 (2003) 935.
[48] W. Fu, W. Deng, H. Saltsburg, M. Flytzani-Stephanopoulos, Appl. Catal. B 56 (2005) 57.
[49] V. Aguilar-Guerrero, B.C. Gates, J. Catal. 260 (2008) 351.
[50] G.R. Bamwenda, S. Tsubota, T. Nakamura, M. Haruta, Catal. Lett. 44 (1997) 83.
[51] P. Kracke, T. Haas, H. Saltsburg, M. Flytzani-Stephanopoulos, J. Phys. Chem. C. 114 (2010) 16401.